Molecular Therapy
Original Article

Systemic delivery of antagomirs during blood-brain barrier disruption is disease-modifying in experimental epilepsy

Cristina R. Reschke,[1,2,3] Luiz F.A. Silva,[1] Vamshidhar R. Vangoor,[4] Massimo Rosso,[1] Bastian David,[5] Brenton L. Cavanagh,[6] Niamh M.C. Connolly,[1,2] Gary P. Brennan,[1,2] Amaya Sanz-Rodriguez,[1,2] Catherine Mooney,[2,7] Aasia Batool,[1] Chris Greene,[8] Marian Brennan,[3] Ronan M. Conroy,[9] Theodor Rüber,[5,10,11] Jochen H.M. Prehn,[1,2] Matthew Campbell,[2,8] R. Jeroen Pasterkamp,[4] and David C. Henshall[1,2]

[1]Department of Physiology & Medical Physics, Royal College of Surgeons in Ireland, Dublin D02 YN77, Ireland; [2]FutureNeuro SFI Research Centre, Royal College of Surgeons in Ireland, Dublin D02 YN77, Ireland; [3]School of Pharmacy and Biomolecular Sciences, Royal College of Surgeons in Ireland, Dublin D02 YN77, Ireland; [4]Department of Translational Neuroscience, UMC Utrecht Brain Center, University Medical Center Utrecht, Utrecht University, 3584 CG Utrecht, the Netherlands; [5]Department of Epileptology, University Hospital Bonn, 53127 Bonn, Germany; [6]Cellular and Molecular Imaging Core, Royal College of Surgeons in Ireland, Dublin D02 YN77, Ireland; [7]School of Computer Science, University College Dublin, Dublin 4, Ireland; [8]Department of Genetics, Trinity College Dublin, Dublin 2, Ireland; [9]Department of Epidemiology and Public Health Medicine, Royal College of Surgeons in Ireland, Dublin D02 YN77, Ireland; [10]Epilepsy Center Frankfurt Rhine-Main, Department of Neurology, Goethe University Frankfurt, 60528 Frankfurt am Main, Germany; [11]Center for Personalized Translational Epilepsy Research (CePTER), Goethe-University Frankfurt, 60528 Frankfurt am Main, Germany

Oligonucleotide therapies offer precision treatments for a variety of neurological diseases, including epilepsy, but their deployment is hampered by the blood-brain barrier (BBB). Previous studies showed that intracerebroventricular injection of an antisense oligonucleotide (antagomir) targeting microRNA-134 (Ant-134) reduced evoked and spontaneous seizures in animal models of epilepsy. In this study, we used assays of serum protein and tracer extravasation to determine that BBB disruption occurring after status epilepticus in mice was sufficient to permit passage of systemically injected Ant-134 into the brain parenchyma. Intraperitoneal and intravenous injection of Ant-134 reached the hippocampus and blocked seizure-induced upregulation of miR-134. A single intraperitoneal injection of Ant-134 at 2 h after status epilepticus in mice resulted in potent suppression of spontaneous recurrent seizures, reaching a 99.5% reduction during recordings at 3 months. The duration of spontaneous seizures, when they occurred, was also reduced in Ant-134-treated mice. *In vivo* knockdown of LIM kinase-1 (Limk-1) increased seizure frequency in Ant-134-treated mice, implicating de-repression of Limk-1 in the antagomir mechanism. These studies indicate that systemic delivery of Ant-134 reaches the brain and produces long-lasting seizure-suppressive effects after systemic injection in mice when timed with BBB disruption and may be a clinically viable approach for this and other disease-modifying microRNA therapies.

INTRODUCTION

Targeting coding and noncoding RNAs offers unprecedented potential for precision therapeutics and disease modification.[1] Among leading strategies is the use of antisense oligonucleotides (ASOs), which are now clinically approved for certain neuromuscular diseases and in trials for other conditions.[1,2] There has been less progress, however, with deployment of ASOs for brain diseases. This is in part due to the blood-brain barrier (BBB) preventing the passage of macromolecules from the systemic circulation into the brain.[3] Overcoming the BBB may be possible using encapsulation techniques or conjugation to cell-penetrant peptides; however, the safety and efficacy of these approaches remain uncertain.

Temporal lobe epilepsy (TLE) is the most common and refractory seizure disorder in adults. Many patients do not achieve seizure freedom with anti-epileptic drugs, and there is an urgent, unmet need for disease-modifying or anti-epileptogenic therapies.[4,5] MicroRNAs (miRNAs) have recently emerged as a potential therapeutic target in epilepsy.[6] They are small noncoding RNAs that post-transcriptionally reduce protein levels via base-pairing to complementary regions in target mRNAs. In the brain, miRNAs are required for cell growth, differentiation, and synaptic plasticity as well as the control of neuroinflammation and apoptosis.[7] Notably, many of these processes are dysregulated in epileptogenesis.[6] Altered miRNA biogenesis has been detected in the hippocampus of patients with epilepsy,[8] and genetic deletion of certain miRNAs leads to neurodegeneration and epilepsy in mice.[9,10]

Received 29 April 2020; accepted 15 February 2021;
https://doi.org/10.1016/j.ymthe.2021.02.021.

Correspondence: David C. Henshall, PhD, Department of Physiology & Medical Physics. Royal College of Surgeons in Ireland, 123 St. Stephen's Green, Dublin D02 YN77, Ireland.
E-mail: dhenshall@rcsi.ie

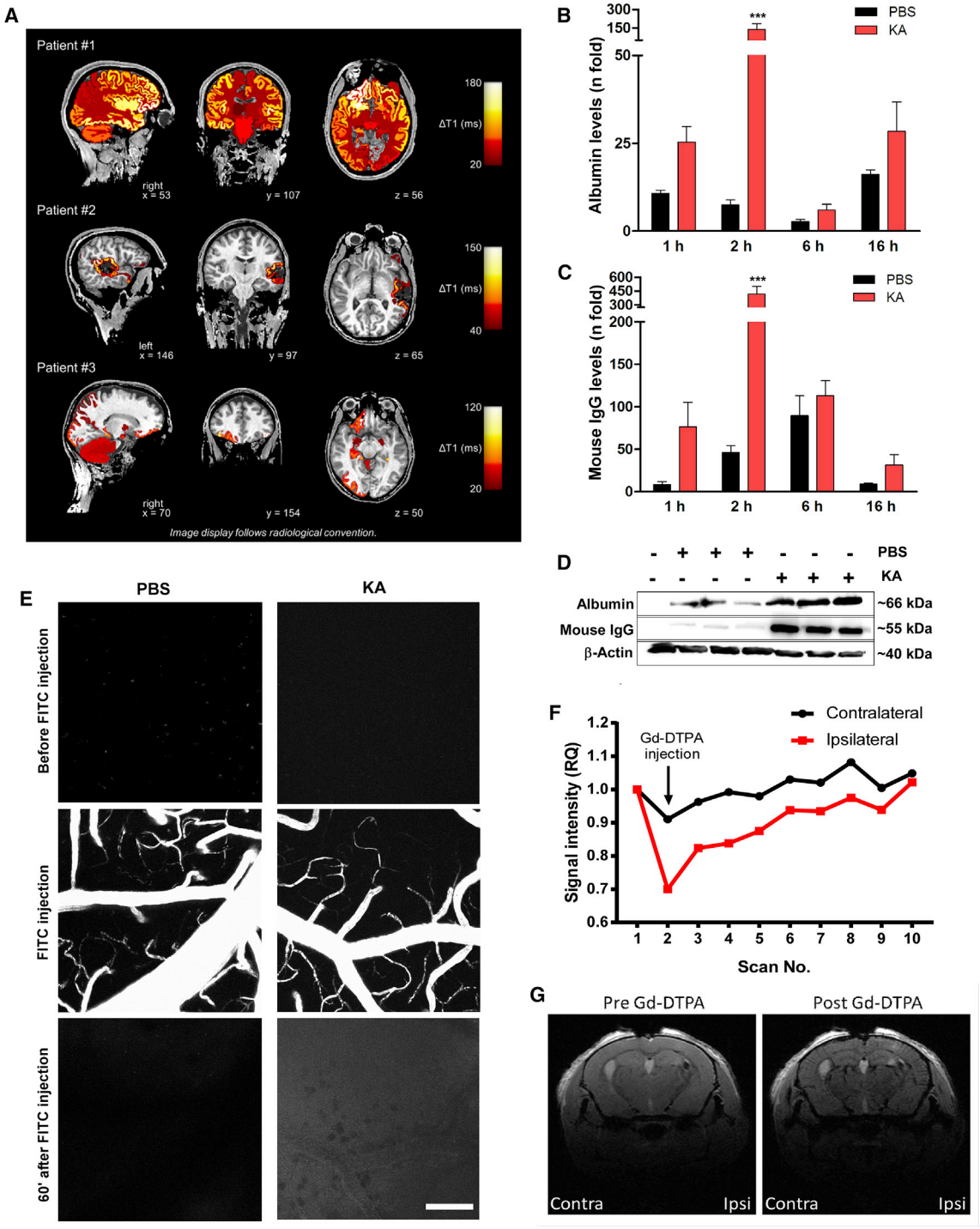

Figure 1. Blood-brain barrier (BBB) disruption in epilepsy patients and after KA-induced SE in mice

(A) BBB dysfunction after seizures in three epilepsy patients undergoing inpatient monitoring as part of their presurgical evaluation (#1, male, 24 years old; #2, male, 34 years old; #3: female, 34 years old). ΔT1 indicates postictal enhancement of gadolinium-based contrast agent. ΔT1 was computed by subtracting postictal quantitative T1 relaxation time maps (qT1) from interictal qT1. Higher ΔT1 values therefore reflect a greater postictal enhancement of contrast agent. ΔT1 values were color-coded and colored labels were superimposed on the anatomical brain volume. Patient #1 showed secondarily generalized tonic-clonic seizure, non-lesional MRI, and ictal EEG onset: right frontal; presumed seizure onset zone: right frontal. Patient #2 showed a focal seizure, MRI: resected cavernoma in left temporal lobe and post-operative epileptic

(legend continued on next page)

Increased brain levels of miR-134-5p (*MIR134*; hereafter, miR-134) has been widely reported in experimental and human TLE.[11–13] miR-134 is a conserved, brain-enriched miRNA that controls dendritic spine morphology via regulation of LIM kinase-1 (Limk-1),[14] a well-characterized serine/threonine kinase that can regulate actin polymerization, although other targets of miR-134 are known.[15,16] Antagomirs are modified ASOs that produce potent and specific inhibition of miRNAs *in vivo*.[1,2,17] Previous studies showed that reducing brain levels of miR-134 protects against evoked seizures in multiple chemoconvulsant models.[11–13,18] Moreover, intracerebroventricular (i.c.v.) injection of miR-134-targeting antagomirs after status epilepticus (SE) produced potent and lasting reductions in the later occurrence of spontaneous recurrent seizures (SRSs) in rodents.[11–13] The mechanism of action is uncertain, although silencing miR-134 *in vivo* produces dendritic spine phenotypes and rescue of protein levels consistent with a mechanism involving de-repression of Limk-1.[11,18]

As with other ASOs, studies have demonstrated that antagomirs do not reach the brain after systemic injection in healthy animals.[19] However, antagomirs targeting miR-134 (Ant-134) might be used therapeutically after acute brain injuries or SE. In this setting, there is likely to be a temporary disruption of BBB integrity.[20–22] We hypothesized that we could deliver Ant-134 to a brain target (hippocampus) after systemic administration if injected concurrent with BBB disruption. In this study, we tracked BBB disruption in a mouse model of SE to inform the timing of systemic delivery of Ant-134. We followed the effects on epilepsy and show potent and lasting suppression of seizure activity and link the mechanism to de-repression of Limk-1.

RESULTS

Impairment of the BBB in humans following seizures

Contrast-enhanced magnetic resonance imaging (MRI) studies have shown temporal and anatomical BBB dysfunction after epilepsy-causing brain injuries[21,22] and seizures[23] in humans. To extend these findings while ascertaining clinical relevance of the systemic delivery of Ant-134, we analyzed contrast-enhanced MRI brain imaging studies of a set of three patients who recently experienced seizures (Figure 1A). Two patients experienced a focal seizure while one patient had a secondary generalized tonic-clonic seizure. A change in ΔT1 indicated postictal enhancement of gadolinium-based contrast agent 25–32 min after seizure onset and injection of contrast agent. The postictal enhancement was anatomically associated with the spread of ictal activity as determined by clinical observation and results of other diagnostic modalities (Figure 1A). These findings provide further evidence for peri-ictal disruption of the BBB occurring after seizures in humans.

Timing and size selectivity of BBB disruption following SE in mice

We first confirmed that Ant-134 does not enter the brain parenchyma after a systemic injection in non-seizure mice (Figure S1A). Thus, we next determined the timing of BBB disruption after experimental SE and whether it is sufficient to allow passage of Ant-134 into the brain after systemic injection. SE was triggered by intraamygdala microinjection of kainic acid (KA) in mice, a well-characterized model of prolonged seizures that involves limbic networks and produces damage to the ipsilateral hippocampus followed by the emergence of SRSs within 3–5 days.[24] The model has proved apt to study anti-epileptogenic therapies and was previously used to study the effects of i.c.v. delivered Ant-134 on SRSs in mice.[11] Although studies have suggested that the model is associated with BBB disruption,[25] the timing and size selectivity of this disruption remain unknown.

We next used immunoblotting to assess the extravasation of serum proteins into brain tissue. Hippocampal samples from saline-perfused naive mice were devoid of the abundant serum proteins albumin (~66 kDa) and immunoglobulin G (IgG; ~150 kDa). Mice that received an intraamygdala injection of vehicle (PBS) presented a slight protein extravasation induced by the surgical procedure (Figures 1B–1D). In contrast, both proteins were readily and highly detected in hippocampal lysates obtained as early as 1 h after SE, consistent with BBB disruption (Figures 1B and 1C). A peak of extravasation was observed at 2 h after SE (Figures 1B–1D). Both albumin and IgG remained detectable in hippocampal lysates at later time points (Figures 1B and 1C).

To determine whether the acute BBB disruption after SE was sufficient to allow passage of a macromolecule the size of Ant-134 (~6 kDa), we used live two-photon imaging through a cranial window to track extravasation of an intravenously (i.v.) injected fluorescein isothiocyanate (FITC)-conjugated 10-kDa dextran tracer around cerebral microvessels in mice (Figure 1E). One week after the surgical procedure to instrument the mice and beginning 1 h after SE, imaging confirmed an FITC signal outside small vessels within the brain ipsilateral to the side of seizure induction, which was not observed in non-seizure, vehicle-injected mice (Figure 1E).

seizures; ictal EEG onset: left temporal; presumed seizure onset zone: left temporal lesion. Patient #3 showed a focal seizure, MRI: focal lesion in right olfactory sulcus; ictal EEG onset: right frontal; presumed seizure onset zone: right olfactory sulcus. (B–G) BBB disruption after KA-induced SE in mice. (B–D) Graphs (data are mean ± SEM) and representative immunoblots (D) show levels (relative to ipsilateral hippocampi of naive mice) of albumin (B) or IgG (C) in the brain after KA or PBS injection. Two-way ANOVA: ***$p < 0.001$. (E) Two-photon images taken 5 min before and 60 min after systemic injection of a 10-kDa FITC-dextran. Note increased intensity 1 h after FITC-dextran injection in SE mice. The z stack images were acquired every 60 s using an upright Carl Zeiss LSM 710 NLO and Zen 2008. A Coherent Chameleon Vision II laser operating at 780 nm with 40.0% laser power (64 MW at sample) and a 500- to 550-nm emission band-pass filter was used for excitation and detection. Scale bar, 100 μm. (F and G) Contrast-enhanced MRI analysis of clearance rates of Gd-DTPA (742 Da) in hippocampal regions after tail vein injection of the contrast agent, 2 h after SE. (F) Graph showing changes in Gd-DTPA clearance between contralateral (contra) and ipsilateral (ipsi) hemispheres (n = 10 for scan replications before and after injection in the same mouse). (G) Representative MRI images depicting ipsilateral and contralateral brain hemispheres before and after Gd-DTPA injection. Data are mean ± SEM.

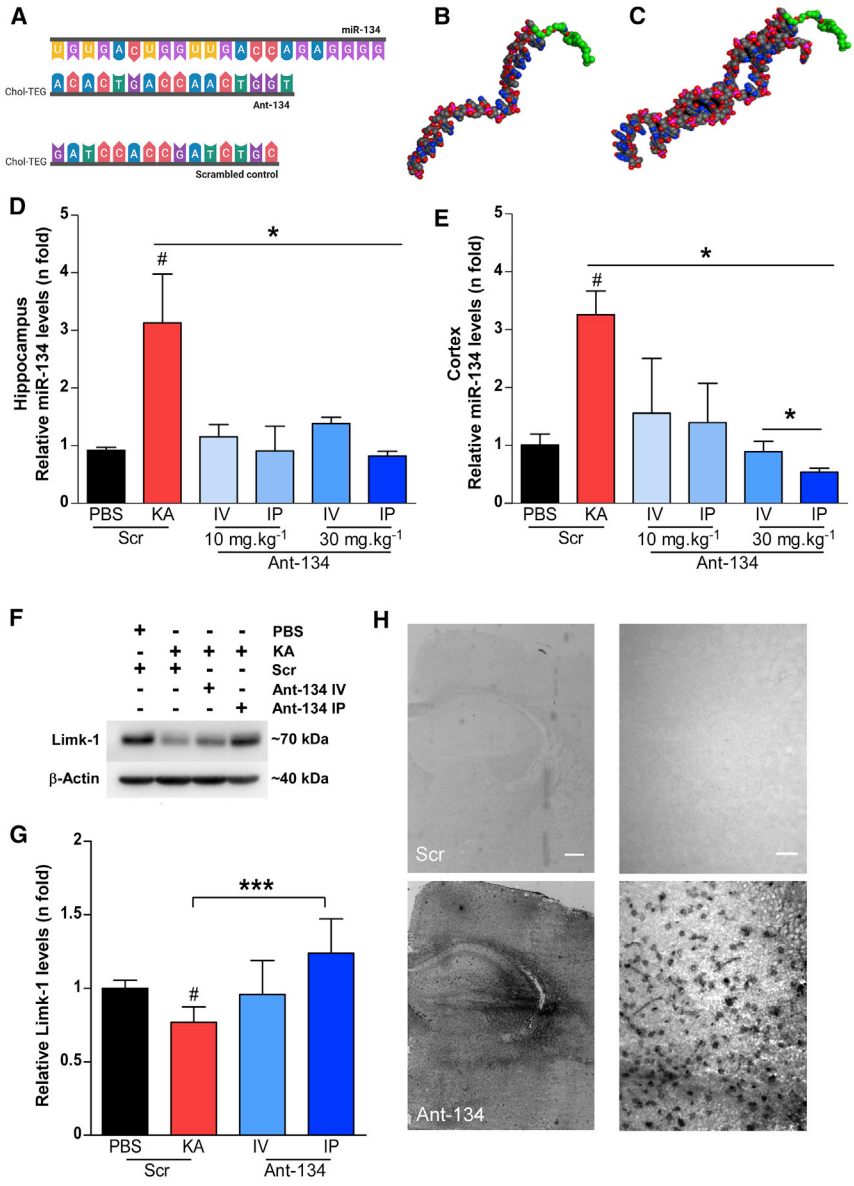

Figure 2. Seizure-facilitated entry of Ant-134 into the mouse brain after systemic injection

(A) Schematic of the ASO sequences of miR-134, Ant-134, and Scr (from top to bottom). (B and C) Predicted models of Ant-134 (B) and the dimer of Ant-134 with miR-134 (C) generated using Molecular Operating Environment, CCG Montreal. Carbon atoms are depicted in gray, oxygen in red, nitrogen atoms in blue, and phosphorous atoms in pink. The carbons in the Chol-TEG (cholesterol moiety via a tetra-ethylene glycol) tag are colored green. (D and E) Levels of miR-134 in the ipsilateral hippocampus (D) and cortex (E) of mice that were systemically injected with Ant-134 or Scr (10 or 30 mg/kg; i.p. or i.v.) at 2 h after KA-induced SE compared to PBS-Scr control mice. ANOVA: *$p < 0.05$ ($n = 3$–6/group). (F and G) Representative immunoblot and graph show Ant-134 (30 mg/kg) systemically administered by i.p. injection prevented the expected reduction of Limk-1 protein levels by KA-induced SE. Data were normalized to β-actin. ANOVA: #$p < 0.05$ compared to PBS, ***$p < 0.001$. (H) Representative images depict the presence of Ant-134 in the mouse brain 24 h after i.p. injection (30 mg/kg; bottom panel). Scr inhibitor probe was used as a negative control. Scale bars represent 400 and 25 μm for original magnifications ×2.5 (left) and ×40 (right), respectively. See also Figures S1A–S1C. Data are mean ± SEM.

Finally, we imaged extravasation of MRI contrast agent[26] in mice 2 h after SE. Using 7-T scanning, we observed enhanced contrast (manifested by an apparent signal disruption based on a T1 flash MRI sequence) within the seizure-damaged hippocampus after systemic gadolinium-diethylenetriamine pentaacetic acid (Gd-DTPA, 800 Da) injection (Figures 1F and 1G). While signal intensity returned to pre-gadolinium levels thereafter, this was delayed on the ipsilateral relative to the contralateral side, reflecting leakage of the gadolinium into surrounding brain tissue (Figure 1G). Therefore, intraamygdala KA-induced SE in mice leads to focal disruption of the BBB sufficient to allow passage of a systemically injected macromolecule such as an antagomir.

Systemic delivery of Ant-134 timed with BBB disruption blocks miR-134 upregulation

We used locked nucleic acid (LNA)-modified cholesterol-tagged antagomirs to achieve potent and specific silencing of miR-134.[11,12] The targeting sequence and a 3D rendering of the predicted structure of Ant-134 and Ant-134 bound to miR-134 are shown in Figures 2A-2C. Two hours after SE, mice were injected either i.v. or intraperitoneally (i.p.) with 10 or 30 mg/kg Ant-134, with dosing guided by previous studies.[17] Control mice were systemically injected with a scrambled LNA-modified ASO (Scr). Brains were removed 24 h later for analysis of miR-134 levels.

Hippocampal (Figure 2D) and neocortical (Figure 2E) levels of miR-134 were ~3-fold higher in mice subject to SE compared to vehicle controls, consistent with previous reports.[11] i.v. and i.p. injection of either 10 or 30 mg/kg Ant-134 blocked the upregulation of miR-134 after SE (Figures 2D and 2E). We next measured levels of the miR-134 target Limk-1 in brain samples from the mice. Consistent with previous reports,[11] protein levels of Limk-1 were lower in hippocampal samples from mice subjected to SE, and this was partly reversed in Ant-134-injected seizure mice (Figure 2F). Notably, target de-repression was greatest in mice given a 30 mg/kg i.p. injection of Ant-134 (Figures 2F and 2G). Based on these findings and the less invasive delivery, an i.p. route was selected for studies thereafter. Then, to confirm that systemically delivered Ant-134 after SE reached the target tissue, we

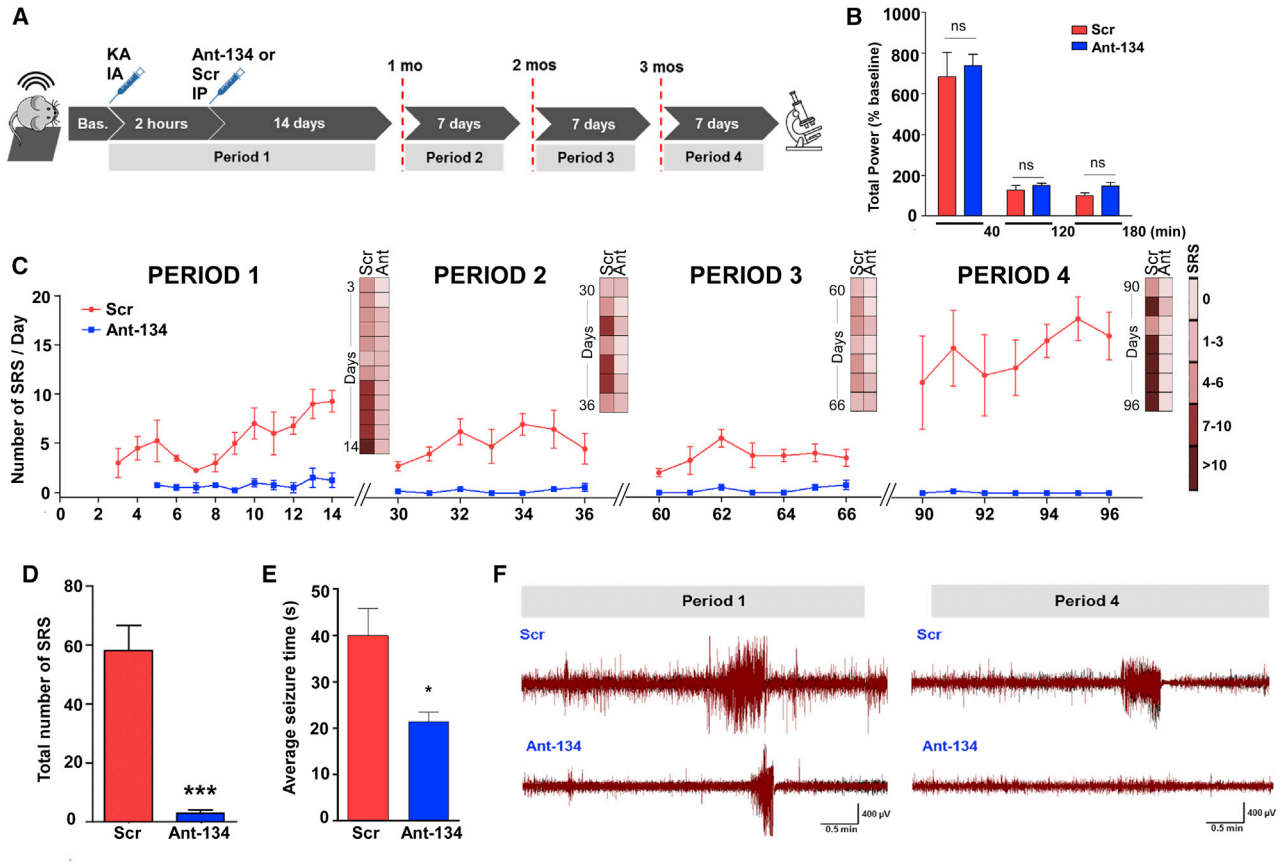

Figure 3. Potent and long-lasting anti-seizure effects of systemic Ant-134 in mice

(A) Experimental design for long-term epilepsy monitoring studies in mice using a telemetric EEG system. After baseline (Bas.) EEG recording, SE was triggered by an intraamygdala (IA) injection of KA and followed by an injection of lorazepam after 40 min. Two hours later, mice were injected with Ant-134 or Scr control (i.p., 30 mg/kg, 10 mL/kg). Continuous EEG data were then collected for 14 consecutive days (sampling epoch called period 1) and again for 7 days at exactly 1 month (period 2), 2 months (period 3), and 3 months (period 4) after SE. (B) No differences (ns, non-significant) were observed in the severity of the KA-induced SE prior to and soon after Ant-134 or Scr injection. The x axis plots time (in minutes) after SE between KA and lorazepam injections; between lorazepam and Ant-134/Scr injection; and up to 1 h after Ant-134 or Scr i.p. injection. (C) Graph shows the number of spontaneous recurrent seizures (SRSs) per day per treatment group over time (periods 1–4), depicting the total number of seizures per group per EEG activation period. (D and E) Graphs show (D) the overall reduction of SRSs (t test; ***$p < 0.001$) and (E) the average duration of SRSs in Ant-134 compared to Scr mice (t test; *$p = 0.042$) covering the entire monitoring period. (F) Representative EEG traces depict SRSs at the last day of recording for period 1 (left) and period 4 (right) for Scr- (top) or Ant-134-treated mice (bottom). Note that the Ant-134 (period 4) EEG trace is similar to Bas. recordings. Data are from n = 5 (Scr) and 6 (Ant-134) (period 1), with the final period data from n = 4 (Scr) and 5 (Ant-134). See also Figures S2A and S2B. Data are mean ± SEM.

performed *in situ* hybridization (ISH) using specific probes for Ant-134 on mouse brain tissue sections collected 24 h after injection. ISH confirmed strong Ant-134 staining within the ipsilateral hippocampus of mice that received an i.p. injection of Ant-134 (30 mg/kg) 2 h after SE (Figure 2H). Images were obtained from the ventral and dorsal hippocampus, and the cellular uptake was quantified (Figures S1B and S1C). The intensity of staining was particularly notable around the CA3 subfield (Figures S1B and S1C), which is the main lesion site and source of SRSs in the model.[27]

Systemic Ant-134 produces potent and lasting suppression of epilepsy in mice

Next, we equipped mice with implantable electroencephalogram (EEG) telemetry units to assess whether systemically delivered Ant-134 affected epilepsy development. Animals were then subjected to SE and, 2 h later, given an i.p. injection of either 30 mg/kg Ant-134 or Scr. Because clinical trials do not use non-targeting ASOs as the placebo arm, we verified that the basic epilepsy phenotype in Scr mice was similar to vehicle (PBS) (Figures S2A and S2B). EEG recording units were activated during SE and for the next 2 weeks. They were then turned off and re-activated for 1 week of recording at 1, 2, and 3 months after SE to assess the permanency of any effects, after which mice were killed and brains processed for histology (see schematic in Figure 3A).

The severity of SE was similar between Ant-134 and Scr groups during the first 3 h after SE, confirming that systemic injection of Ant-134 did not alter epileptiform EEG parameters or the initial

precipitating injury (Figure 3B). Epilepsy monitoring in freely moving Scr-treated mice determined that SRSs emerged within 3–4 days of SE, consistent with the known course of epilepsy in the model.[11] During the first 2-week recording period, SRSs occurred daily in most Scr mice, ranging from 1 to 20 per day (Figure 3C). In contrast, mice given a systemic injection of Ant-134 after SE displayed only rare seizures during the first 2-week recording period and these emerged slightly later (at 5–7 days) (see period 1 in Figures 3C and 3D). In the first 2 weeks of monitoring, we observed ~85% fewer SRSs in Ant-134-injected mice compared to Scr-injected mice (period 1; Figures 3D and 3E). A secondary measure of seizure burden, based on summing together the duration of all seizures, revealed an ~92% reduction in Ant-134-injected mice when compared with Scr-injected mice.

Ant-134-injected mice continued to display dramatically lower rates of SRSs compared to Scr mice during monitoring at 1, 2, and 3 months after SE (see periods 2, 3, and 4, respectively, in Figures 3C and 3F) and presented an overall average of 6.14 (out of 7) days seizure-free (see periods 2–4). Most notably, during the final week of seizure monitoring at the 3-month time point, only a single SRS was detected in one of the Ant-134 mice compared to an average of ~100 epileptic seizures per mouse in the Scr group (period 4; Figures 3C and 3F). This was equivalent to a 99.5% lower seizure rate in Ant-134 mice in the third month, and around 93.4% over all periods. On average, the duration of SRSs was ~45% shorter in Ant-134-injected than in Scr-injected mice during all monitoring periods (Figure 3E).

Histological findings in Ant-134-treated mice

Brains from mice obtained at the end of EEG monitoring (i.e., 3 months after SE) displayed modest hippocampal atrophy and were macroscopically similar between Ant-134- and Scr-injected mice (Figure 4). However, tissue sections from Ant-134-treated mice displayed lower glial fibrillary acid protein (GFAP) staining when compared to Scr, suggestive of reduced astrogliosis (Figures 4A and 4E). Counts of Iba1-positive cells, likely microglia, were not different between the groups (Figures 4B and 4E). Gross neuron loss was similar between groups (Figure 4D), as assessed using a semi-quantitative scoring system, but Ant-134-treated mice had higher numbers of inhibitory parvalbumin interneurons[28] (Figures 4C and 4E).

We used additional brain tissue sections from the post-monitoring mice to stain for Ant-134. The absence of the antagomir at the end of epilepsy monitoring would support a disease-modifying effect. Ant-134 staining was readily observed at 24 h after SE from mice injected with Ant-134 (also see Figure 2H) whereas Ant-134 staining was not detectable in the brain tissue sections from mice at the end of epilepsy monitoring (Figure 4F). Therefore, the lack of SRSs in Ant-134 mice was unlikely to be due to the continuing presence of Ant-134 within the brain. To support these histological findings, additional Ant-134- and Scr-treated mice at 2 h after SE were generated and brains obtained at 1 month for measurement of miR-134. These results revealed that silencing of miR-134 was no longer detectable (Figure S3A).

In vivo evidence for anti-seizure mechanism of Ant-134

We next explored the mechanisms by which Ant-134 produces anti-seizure effects. Limk-1 has a direct role in the control of dendritic structure and function,[14] and Ant-134 restores Limk-1 levels after SE[11] (and see Figures 2F and 2G). We therefore hypothesized that the seizure-suppressive effects of Ant-134 may be due in part to de-repression of Limk-1. Accordingly, lowering Limk-1 levels should revert the anti-seizure phenotype. To target Limk-1, we used LNA-gapmer ASOs, which deplete target mRNAs via an RNase H-dependent mechanism (see Figure 5A). We first performed *in vitro* screening to identify an optimal sequence that reduced Limk-1 levels by an amount equivalent to that found to be recovered by Ant-134 treatment (data not shown). The ability of an i.c.v. injection of gapmer to knock down Limk-1 was then confirmed *in vivo* (Figure 5B). Next, we equipped mice for EEG telemetry recordings. One group of mice then received i.c.v. injections of gapmer while the other group received its scrambled version, and all mice were injected with Ant-134 (30 mg/kg i.p.) 2 h after SE. Gapmer injections were repeated every second day. SRS frequency was quantified as before for a period of 2 weeks (see schematic in Figure 5A). Injection of gapmer alone did not produce epilepsy in mice (data not shown).

As expected, the frequency of SRSs was very low in mice given systemic Ant-134 after SE and i.c.v. injections of the non-targeting gapmer (Figures 5C and 5D). The frequency of SRSs in Ant-134-treated SE mice given Limk-1 gapmer was higher within a few days, reaching a frequency similar to the standard model (i.e., average of four to six SRSs per day) (Figures 5C and 5D). Thus, reducing Limk-1 levels *in vivo* partly obviates the anti-seizure phenotype of Ant-134, supporting de-repression of Limk-1 in the anti-seizure mechanism of Ant-134. However, underscoring the challenge of linking the mechanism of Ant-134 exclusively to Limk-1, we found similar levels of Limk-1 in hippocampal samples of Ant-134- or Scr-injected mice 1 month after SE (Figure S3B).

Based on these findings and the known multi-targeting effects of miRNAs, we sought to identify other potential targets altered by Ant-134, performing transcriptional profiling of the hippocampus of mice 24 h after SE. This identified 39 differentially expressed mRNAs between Scr- and Ant-134-treated mice (Table S1; Figure 5E). Interestingly, pathway enrichment analysis highlighted several processes involving *Kcnj10* and *Kcnj16*, inward-rectifying potassium channel subunits, and also in γ-aminobutyric acid (GABA) signaling (Figure 5F). Indeed, the loss of *KCNJ10* may cause epilepsy in humans.[29] Additional pathways altered by Ant-134 include the synthesis of prostaglandins (PGs) and thromboxanes (TXs), specifically the hematopoietic PGD synthase (*Hpgds*) and the brain PGD2 synthase (*Ptgds*). Notably, these pathways modulate seizures and seizure-induced neuronal death.[30–32] Taken together, the significant upregulation of these mRNAs support additional seizure suppressive and neuroprotective mechanisms mediated by Ant-134.

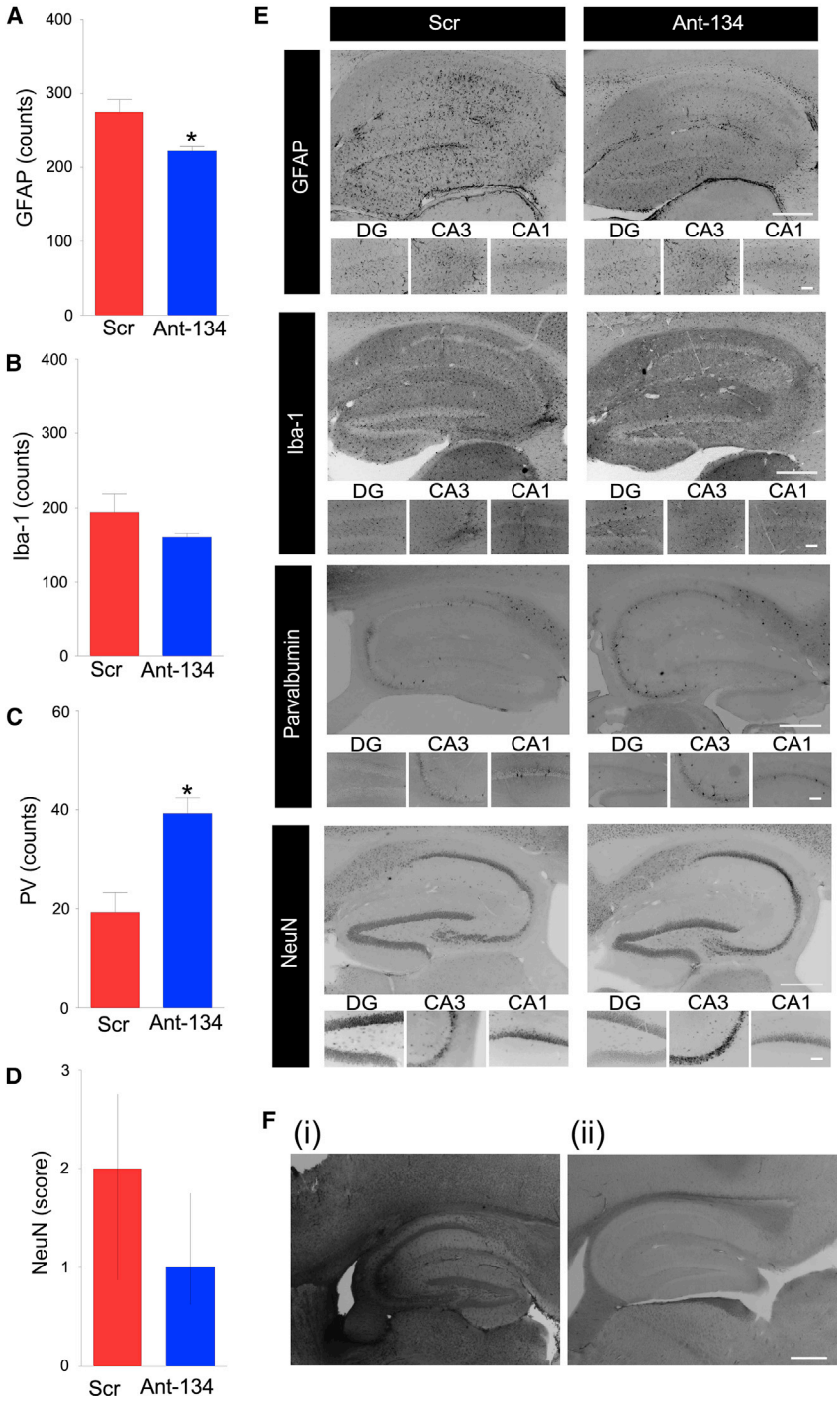

Figure 4. Histological findings in Ant-134-treated mice

(A–E) Graphs (A–D) and representative images (E) of brains obtained at the end of long-term epilepsy monitoring stained for (A) GFAP (astrocytic marker), (B) Iba-1 (microglia), (C) parvalbumin (PV; a marker for GABAergic interneurons), and (D) NeuN (broad neuronal marker). Positive cells were quantified per hippocampal subfield and were the average of two adjacent sections by an observer blinded to the experimental treatment. n = 4 (Scr), n = 5 (Ant-134). *$p < 0.05$ compared to Scr. Neuronal damage (NeuN) was assessed based on a graded 5-point system under ×40 magnification: level 0, no damage; level 1, 0%–25%; level 2, 25%–50%; level 3, 50%–75%; level 5, 75% or more cell loss. (E) Representative images of each cellular marker show the whole ipsilateral hippocampus (original magnification, ×5; top) and hippocampal sub-regions (DG, CA3, and CA1; original magnification, ×20; bottom). (F) Representative ISH images depict (i) Ant-134 signal in the brain at 24 h after SE in a mouse injected with Ant-134, and (ii) the lack of Ant-134 signal in the brain of an Ant-134-injected SE mouse at the end of epilepsy monitoring. Scale bar represents 400 μm for original magnifications of ×2.5. Data are mean ± SEM except in (D), which are median and interquartile range.

DISCUSSION

The targeting of miRNAs has emerged as a promising therapeutic approach for drug-resistant epilepsy, but the clinical deployment of miRNA-blocking ASOs is limited by the need to circumvent the BBB. The present study demonstrates that, when timed with BBB disruption after SE, a single systemic injection of an antisense miRNA inhibitor produces potent and lasting suppression of TLE in mice. These findings expand the evidence for the disease-modifying potential of antagomirs targeting miR-134 and offer a clinically viable route for delivery of this promising experimental therapy for epilepsy.

Targeting miR-134 using ASOs has been particularly notable for the potency and disease-modifying actions demonstrated across different *in vivo* animal models.[11–13,18] Delivering ASOs to the brain is a key challenge, however, as is elucidating the mechanism of action because the multi-targeting actions of miRNAs raise safety concerns.[6] Currently, delivery of ASOs for brain diseases is expected to require an intrathecal or i.c.v. route, or some form of conjugation or encapsulation technique. However, BBB disruption accompanies many epilepsy-triggering brain injuries,[21] potentially facilitating non-invasive (i.e., systemic) delivery. The present study addressed both delivery and mechanism of action, revealing that systemic injection of Ant-134 can prevent SRSs in experimental epilepsy, principally through a single target.

While prolonged or repeated seizures are known to cause disruption of the BBB, the focus until now has been on understanding how this

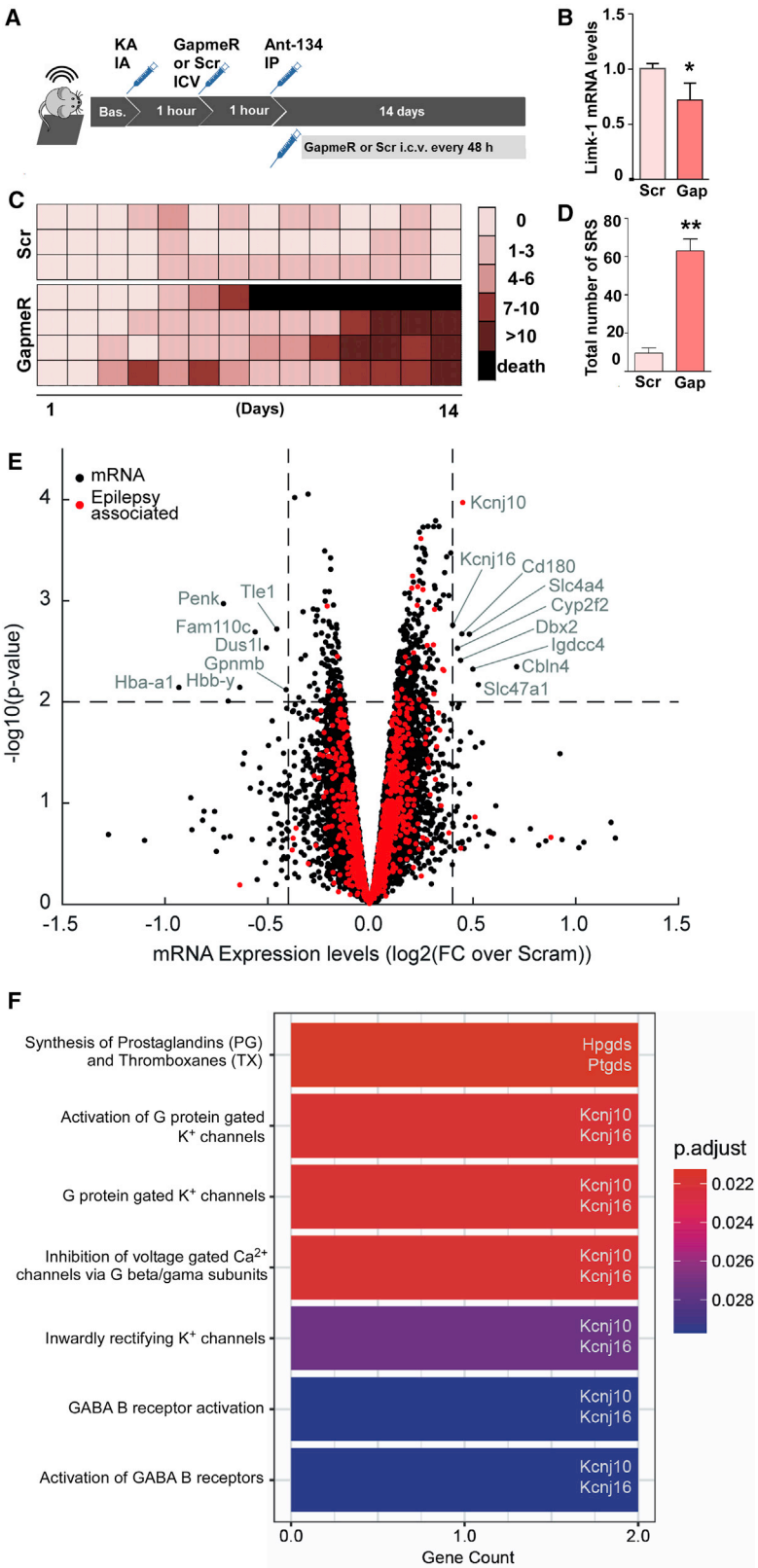

Figure 5. Molecular effects and mechanism of Ant-134

(A) Mice were equipped with telemetry devices, underwent intra-amygdala KA-induced SE, and 1 h later were intracerebroventricularly (i.c.v.) injected with the first dose of an ASO gapmer to silence *Limk-1* mRNA (called Gap; n = 4; 0.01 nmol/2 μL) or its scramble negative control (called Scr; n = 3; 0.01 nmol/2 μL). One more hour after (2 h after SE), all mice were systemically injected with Ant-134 (30 mg/kg, i.p.). Long-term EEG was continued for 2 weeks, and mice received i.c.v. doses of gapmer or Scr every 48 h for the overall recording time (total of seven administrations on experimental days 1, 3, 5, 7, 9, 11, and 13). (B) Reduction of Limk-1 mRNA in the mouse hippocampus 24 h after a single gapmer injection in comparison with Scr control (n = 3/group; t test; *$p < 0.05$). (C) Individual SRS counts per day for Ant-134 mice that received either gapmer or Scr. Each line represents data from the same mouse over time, and each row represents the seizure counts for the respective day of EEG recording. (D) Total number of SRSs over 2 weeks of EEG recordings comparing Ant-134 + Scr mice to Ant-134 + gapmer mice (n = 3/group; the mouse that died was excluded for statistical purposes; t test; **$p = 0.013$). (E) Microarray analysis showing gene expression changes 24 h after KA-induced SE in a separate group of mice treated i.p. with Ant-134 or Scr (n = 3/group). Note the selected differential expression induced by Ant-134. Dashed lines are drawn at $\log_2$FC (fold change) of 0.4 and −0.4 (equivalent to ± 1.3-FC) and $-\log_{10}$(p value) of 1.3 (equivalent to FDR p value of 0.05). mRNA with $-\log_{10}$(p value) >2.0 and $\log2_{FC}$ >0.4 or less than −0.4 are labeled, and those identified as associated with epilepsy are marked in red. For mRNA with multiple isoforms, we selected the maximal p value and associated FC. Three mRNA (Hba-a2, Hbb-b1, Hbb-b2) with $\log_2$FC less than −1.5 were removed from the plotted results for clarity. (F) Significantly enriched Reactome pathways for the mRNAs labeled in (E) (adjusted p value [p.adjust] < 0.05). Each enriched pathway contains two mRNAs from the input list, as highlighted on the right of the bars. Data are mean ± SEM.

contributes to epilepsy.[20,23] In this study, we asked whether BBB disruption after SE could be appropriated to deliver a systemically administered antagomir to treat epilepsy. Using multiple assessments of BBB integrity, including extravasation of plasma markers and live brain imaging, we identified a disruption 2 h after SE sufficient to allow passage of systemically administered Ant-134 into the brain parenchyma. While the upper size limit of this disruption was not pursued, the selectivity size and timing align with earlier histological and biochemical findings in the same model,[25] as well as results in other models of SE.[20] We focused on i.v. and i.p. routes for delivering Ant-134 to the brain, although other minimally invasive routes (e.g., subcutaneous) and either earlier or later time points for injection may also be effective. Target engagement after systemic injection was confirmed by measurement of miR-134 knockdown and increased Limk-1 and demonstrated by staining for the antagomir in the damaged CA3 subfield, a key site of ictogenesis during SRSs in the model.[27] However, delivery to other sites may also be important.[4] Indeed, BBB disruption is not restricted to the hippocampus in the model, and we observed knockdown of miR-134 by Ant-134 in the neocortex after systemic delivery.

Our data from long-term epilepsy monitoring revealed remarkable disease-modifying effects of silencing miR-134 using systemically delivered Ant-134 after SE. Seizures were reduced by 99.5% during the final week of monitoring at 3 months. This exceeds the performance of other anti-epileptogenic approaches currently under investigation.[5] The anti-seizure effect was also somewhat superior to the outcome when Ant-134 was delivered by the i.c.v. route in the same model, perhaps due to differences in the amount of Ant-134 that reached brain sites,[11,13] including the contralateral hippocampus,[24] or the timing of Ant-134 delivery, which was slightly later in the present study.[11,13] Interestingly, miR-134 silencing lasted longer after a single i.c.v. injection[11] than after the single systemic administration. Appraisal of how these individual variables affect performance may yield further improvements in effectiveness. Further studies are needed to determine whether Ant-134 can prevent SRSs following epileptogenic insults besides SE.[21,22]

The multi-targeting nature of miRNAs makes understanding the mechanism(s) by which their inhibition produces anti-seizure effects uniquely challenging.[33] Past studies showed that miR-134 targets Limk-1, a protein that promotes dendritic spine expansion by regulating actin dynamics through phosphorylation of cofilin.[14,18] In this study, we used gapmer ASOs to produce a partial reduction in Limk-1 levels, an approach that is physiologically relevant to the scale of protein suppression by a miRNA on a target.[7,14] This was sufficient to increase SRSs in Ant-134-treated epileptic mice, providing *in vivo* support for the disease-modifying effects being a result of de-repression of Limk-1. This implies that the anti-seizure effects of Ant-134 could result from adjustment to synaptic microstructure, perhaps curtailing the capacity of neuronal networks to propagate hypersynchronous discharges.[34] The finding fits with an emerging view that some miRNAs produce strong effects on single targets, perhaps because of spatial co-localization.[35] Notably, other antagomirs with anti-seizure effects have been reported to derive effects from de-repression of single ion channels.[33] Nevertheless, Limk-1 inhibition did not fully obviate the anti-seizure effects of Ant-134 within 2 weeks after SE. Moreover, Limk-1 levels were restored at 1 month after SE followed by Ant-134 treatment. Taken together, it suggests that other targets of miR-134 may contribute to the observed phenotype or pathophysiology. On this note, we observed reduced astrogliosis and sparing of interneurons in brain sections from Ant-134 mice, both of which could account for reduced seizures,[28,36] but could also be a consequence of fewer seizures. The presence of extensive neuronal changes and gliosis and the profound changes in seizure frequency over time precluded an assessment of spine structure in this study. Our profiling of the hippocampal transcriptional landscape in Ant-134-treated mice identified further potential targets that might be explored, including potassium channels and the synthesis of PGs. Studies in human cells or tissues will also be needed to assure clinical relevance of the Ant-134 mechanism and target pool.

The present findings improve the prospects for the development of an antagomir therapy for epilepsy. An antagomir therapy has already completed clinical trials for hepatitis C,[37] and various others are in development, and ASO-based treatments are in clinical use for neuromuscular diseases.[1] Although pharmacokinetic and toxicity studies have not yet been performed, broad safety might be assumed on the basis that mice in our study were given a systemic injection of Ant-134 and lived for 3 months. This may be helped by the largely CNS expression of miR-134,[14] which is specifically expressed by neurons. While manipulation of a miRNA that regulates dendritic spines carries risks, Ant-134 injections in mice[11,18] and rats[34] were not reported to impact hippocampal function or animal behavior.

How might an Ant-134 therapy be tested in patients? The closest clinical scenario to the studies here would be deployment of the antagomir to prevent the development of epilepsy in at-risk individuals. Such a trial would require, however, the identification of biomarkers of human epileptogenesis.[5] Although validated biomarkers do not yet exist, increased miR-134 levels in biofluids including plasma have been reported in some epilepsy patients,[38] and the co-development of devices for point-of-care miRNA testing could further enable translation.[39] However, preclinical studies show that Ant-134 can prevent SRSs in rats that underwent the perforant-pathway stimulation model in which miR-134 is not dysregulated.[12] We have also shown that Ant-134 reduces seizures in the pilocarpine[18] and the pentylenetetrazole[12] models. Although we recognize that before translation the molecule should be tested for effects in already-established epilepsy, a first clinical trial could instead focus on testing in pharmacoresistant focal epilepsy. An intracerebral injection might be offered to patients awaiting neurosurgery such that the target tissue would be excised later and studied for antagomir effects, as proposed for gene therapy trials for this patient group.[40] Finally, although we took advantage of the BBB disruption that accompanies prolonged seizures, other methods for artificially opening the BBB may also facilitate delivery of Ant-134 in patients such as hyperosmotic treatments or ultrasound.

In summary, the present study shows that timed systemic delivery of Ant-134 produces potent and long-lasting disease-modifying effects that are partly mediated by Limk-1. These findings suggest that this miRNA-based therapy can be delivered using a clinically relevant route, and they provide the rationale for pursuing further pre-clinical and clinical studies, which are needed to evaluate the safety and efficacy of this potential candidate for the treatment of epilepsy.

MATERIALS AND METHODS

MRI in epilepsy patients

The study was reviewed and approved by the local Institutional Review Board of the Medical Faculty of the University of Bonn (116/19) and all patients provided written informed consent. Three epilepsy patients undergoing in-patient monitoring at the University of Bonn Medical Center were postictally and interictally scanned in a 3-T Magnetom Trio (Siemens Healthineers) applying quantitative MRI, as before.[23]

Antagomir treatment and EEG recordings in mice

Adult male C57BL/6-OlaHsd mice (~7 weeks old) were housed in accordance with the European Communities Council Directive (2010/63/EU), the NIH *Guide for the Care and Use of Laboratory Animals*, and following ARRIVE guidelines on a 12-h light/12-h dark cycle with standard food and water available *ad libitum*. All animal experiments were approved by the Research Ethics Committee of the Royal College of Surgeons in Ireland (RCSI; REC-842), under licenses from the Health Products Regulatory Authority (AE19127/001 and AE19127/P057), Dublin, Ireland. Sample sizes were defined based on our previous work,[11] approved by a biostatistician, and not altered during or after study completion.

Treatment groups were randomly and blindly assigned before the induction of SE. Ant-134 (anti-mmu-miR-134; molecular weight [MW], 6,127.3 Da) or Scr control (Exiqon, LNA-modified and 3′-cholesterol-modified oligonucleotides) in sterile PBS (pH adjusted to 7.4) was prepared at a concentration of 7.5 mg/mL and injected i.v. or i.p. at 10 or 30 mg/kg in mice at 2 h after intra-amygdala KA-induced SE. Stereotaxic-guided surgical procedures were performed a week prior to KA-induced SE and EEG recordings, as described.[11] Acute and long-term EEG assessments were performed using Xltek (Natus) and Data Sciences International (DSI) telemetry (F20-EET) systems, respectively. The telemetry EEG epochs were collected (Ponemah v6.30 software; DSI) for 2 weeks after SE (period 1) and for 1 week at exactly 1, 2, and 3 months after SE (periods 2, 3 and 4, respectively) and manually analyzed. Statistical correction was applied for animals that were seizure-free at certain days or died during the monitoring. SE was defined as at least 5 min of continuous seizure activity, and seizures as high-frequency (>5 Hz), high-amplitude (>2× baseline) polyspike discharges of ≥5-s duration. SRSs were defined as a clear, bi-directional ictal event comprising of a sudden, repetitive, evolving stereotyped waveform, >2× baseline with a definite start, middle, and end and lasting for at least 10 s.

Limk-1 silencing in mice

Mice underwent intra-amygdala KA-induced SE under long-term EEG, and 1 h later were injected with the first dose of an ASO gapmer to silence Limk-1 mRNA (0.01 nmol/2 μL, i.c.v.) or Scr control. At 2 h after SE, all mice were systemically injected with Ant-134 (30 mg/kg, i.p.), and EEG was continued for 2 weeks. Mice received in total seven i.c.v. doses of gapmer or Scr, spaced 48 h apart, for the overall recording time.

Live imaging in mice: two-photon microscopy and MRI

The BBB opening was imaged by tracking extravasation of a systemically injected tracer in mice after intraamygdala KA or PBS injections. Mice were equipped with a 5-mm cranial window and a week later FITC-dextran was injected (10 kDa; i.v.; 40 mg/kg) and extravasation was monitored by two-photon microscopy from 1 h after the intraamygdala injections. At 2 h after KA or PBS, mice were injected a second time with FITC and the cumulative extravasation was observed.

High-resolution T1-weighted MR images (resolution, 0.156 × 0.156 × 5 mm^3; field of view, 20 × 20 × 17.9 mm^3; matrix, 128 × 128 × 30; repetition time/echo time (TR/TE), 500/2.7 ms; flip angle, 30°; number of averages, 3; acquisition time, 2 min 24 s; repetitions, 12) were acquired 2 h after SE before and after tail vein injection of 100 μL of a 1:3 dilution of Gd-DTPA (0.5 M stock solution, Bayer) using a dedicated small rodent 7-T MRI system.[25] Both analyses were performed using Fiji.[26,41]

Transcriptome and protein analysis

Total RNA was isolated from ipsilateral cortex or hippocampus samples. Limk-1 transcripts and miR-134 levels were analyzed by SYBR Green-based quantitative real-time PCR (1 μg of total RNA) and TaqMan assays (250 ng of RNA), respectively,[11] and miR-134 mRNA targets were analyzed by microarray (3 μg of total RNA). Microarrays used were Mouse Whole Genome GE 4×44K v1 (Agilent Technologies) representing 41,174 *Mus musculus* 60-mer probes in a 4×44K layout, as described.[42] Actin (for mRNA qPCR) or RNU19 (for miRNA TaqMan) were used for normalization and relative fold change determined using the ΔΔCT method.[11] After automated data extraction (ImaGene 8.0, BioDiscovery), microarray data were normalized on mean spot intensities (by Loess), and gene-specific dye bias was corrected based on a within-set estimate. Differential expression p values (Benjamini-Hochberg false discovery rate [FDR] correction) were calculated using the limma package in R v2.12. Primer sequences for qPCR were the same as before.[11] The extravasation of albumin and IgG into the brain parenchyma[25] or the effects of Ant-134 on Limk-1 levels[11] after SE were assessed by western blotting as before.[11] Images were captured using a Fujifilm LAS-400, and densitometry was performed using AlphaEaseFC4.0 gel-scanning integrated optical density software (Alpha Innotech). KA + Scr i.p. and i.v. were grouped for statistical purposes. Microarray data are available at the Gene Expression Omnibus (GEO: GSE166097).

Reactome pathway enrichment analysis

Reactome[43] pathway enrichment analysis (pathways with 10–500 genes) was performed in R version 4.0.2,[44] using ReactomePA[45] and clusterProfiler[46] packages, with an adjusted p value (Benjamini-Hochberg) cutoff of 0.05.

In situ hybridization and immunohistochemistry

Detection of Ant-134 by non-radioactive *in situ* hybridization (ISH) and immunohistochemistry was performed on free-floating coronal sections obtained either at 24 h after SE or after long-term EEG telemetry experiments.[11] Hybridization was performed using a 5 nM double-digoxigenin (DIG) (3′ and 5′)-LNA probe for a 134-inhibitor probe (Exiqon) or an LNA-DIG scramble inhibitor probe. The cellular uptake mean ratio was calculated as per the formula described by Vuokila et al.[47] for each region of interest (ROI). Sections for immunohistochemistry were incubated with primary antibody (NeuN, GFAP, Iba-1, or parvalbumin; all from Cell Signaling Technology) and fluorescently labeled secondary antibodies (Alexa Fluor 488 or 546). Quantification was performed as before.[48]

Data availability

All data associated with this study are available in the main text, and microarray data are deposited in GEO: GSE166097.

SUPPLEMENTAL INFORMATION

Supplemental Information can be found online at https://doi.org/10.1016/j.ymthe.2021.02.021.

ACKNOWLEDGMENTS

The authors would like to thank Eva Jimenez-Mateos and Tobias Engel for advice on technical aspects. This work was supported in part by a research grant from Science Foundation Ireland (SFI) under grant no. 16/RC/3948 and co-funded under the European Regional Development Fund and by FutureNeuro industry partners. The authors also acknowledge funding from the Health Research Board Ireland (HRA-POR-2013-325 to D.C.H.) and Science Foundation Ireland (13/IA/1891 and 11/TIDA/B1988 to D.C.H.; 17/TIDA/5002 to C.R.R.; SFI/14/ADV/RC2721 to C.M.) and fellowships from the Brazilian National Council for Scientific and Technological Development (CNPq; to L.F.A.S.); the Dutch Epilepsiefonds (WAR 12-08 and WAR 15-05 to R.J.P.); the Irish Research Council (to C.R.R.); CURE Epilepsy (to D.C.H. and C.R.R.); and from the European Union Seventh Framework Programme (FP7/2007-2013) under grant agreement no. 602130 (EpimiRNA).

AUTHOR CONTRIBUTIONS

C.R.R. performed *in vivo* studies and EEG analysis. L.F.A.S. performed immunohistochemistry and analysis. V.R.V. and R.J.P. performed *in situ* hybridization and microarray assays. M.R., C.R.R., and A.S.-R. performed *in vitro* characterization of gapmers. B.D. and T.R. performed and analyzed human MRI. B.L.C. and C.R.R. performed two-photon microscopy. N.M.C.C., C.M., and J.H.M.P. performed bioinformatics analysis. G.P.B. and A.S.-R. performed and analyzed qPCRs and western blotting for miR-134 and Limk-1. A.B. and C.R.R. performed albumin and mouse IgG western blotting. C.G. and M.C. performed the MRI imaging in mice. M.B. performed the Ant-134 structure 3D modeling and predictions. R.M.C. assisted with experimental design and statistical analysis. C.R.R. and D.C.H. conceived and designed the study, and D.C.H. wrote the initial manuscript. All authors contributed to and approved the final manuscript.

DECLARATION OF INTERESTS

D.C.H. reports patent US9803200 B2 "Inhibition of microRNA-134 for the treatment of seizure-related disorders and neurologic injuries," and D.C.H. and C.R.R. report patent WO2019219723A1 "Pharmaceutical compositions for treatment of microRNA related diseases." The remaining authors declare no competing interests.

REFERENCES

1. Levin, A.A. (2019). Treating disease at the RNA level with oligonucleotides. N. Engl. J. Med. *380*, 57–70.
2. Khorkova, O., and Wahlestedt, C. (2017). Oligonucleotide therapies for disorders of the nervous system. Nat. Biotechnol. *35*, 249–263.
3. Obermeier, B., Daneman, R., and Ransohoff, R.M. (2013). Development, maintenance and disruption of the blood-brain barrier. Nat. Med. *19*, 1584–1596.
4. Devinsky, O., Vezzani, A., O'Brien, T.J., Jette, N., Scheffer, I.E., de Curtis, M., and Perucca, P. (2018). Epilepsy. Nat. Rev. Dis. Primers *4*, 18024.
5. Löscher, W. (2020). The holy grail of epilepsy prevention: preclinical approaches to antiepileptogenic treatments. Neuropharmacology *167*, 107605.
6. Henshall, D.C., Hamer, H.M., Pasterkamp, R.J., Goldstein, D.B., Kjems, J., Prehn, J.H.M., Schorge, S., Lamottke, K., and Rosenow, F. (2016). MicroRNAs in epilepsy: pathophysiology and clinical utility. Lancet Neurol. *15*, 1368–1376.
7. McNeill, E., and Van Vactor, D. (2012). MicroRNAs shape the neuronal landscape. Neuron *75*, 363–379.
8. McKiernan, R.C., Jimenez-Mateos, E.M., Bray, I., Engel, T., Brennan, G.P., Sano, T., Michalak, Z., Moran, C., Delanty, N., Farrell, M., et al. (2012). Reduced mature microRNA levels in association with dicer loss in human temporal lobe epilepsy with hippocampal sclerosis. PLoS ONE *7*, e35921.
9. Hébert, S.S., Papadopoulou, A.S., Smith, P., Galas, M.C., Planel, E., Silahtaroglu, A.N., Sergeant, N., Buée, L., and De Strooper, B. (2010). Genetic ablation of *Dicer* in adult forebrain neurons results in abnormal tau hyperphosphorylation and neurodegeneration. Hum. Mol. Genet. *19*, 3959–3969.
10. Tan, C.L., Plotkin, J.L., Venø, M.T., von Schimmelmann, M., Feinberg, P., Mann, S., Handler, A., Kjems, J., Surmeier, D.J., O'Carroll, D., et al. (2013). MicroRNA-128 governs neuronal excitability and motor behavior in mice. Science *342*, 1254–1258.
11. Jimenez-Mateos, E.M., Engel, T., Merino-Serrais, P., McKiernan, R.C., Tanaka, K., Mouri, G., Sano, T., O'Tuathaigh, C., Waddington, J.L., Prenter, S., et al. (2012). Silencing microRNA-134 produces neuroprotective and prolonged seizure-suppressive effects. Nat. Med. *18*, 1087–1094.
12. Reschke, C.R., Silva, L.F.A., Norwood, B.A., Senthilkumar, K., Morris, G., Sanz-Rodriguez, A., Conroy, R.M., Costard, L., Neubert, V., Bauer, S., et al. (2017). Potent anti-seizure effects of locked nucleic acid antagomirs targeting miR-134 in multiple mouse and rat models of epilepsy. Mol. Ther. Nucleic Acids *6*, 45–56.
13. Gao, X., Guo, M., Meng, D., Sun, F., Guan, L., Cui, Y., Zhao, Y., Wang, X., Gu, X., Sun, J., and Qi, S. (2019). Silencing microRNA-134 alleviates hippocampal damage and occurrence of spontaneous seizures after intraventricular kainic acid-induced status epilepticus in rats. Front. Cell. Neurosci. *13*, 145.
14. Schratt, G.M., Tuebing, F., Nigh, E.A., Kane, C.G., Sabatini, M.E., Kiebler, M., and Greenberg, M.E. (2006). A brain-specific microRNA regulates dendritic spine development. Nature *439*, 283–289.
15. Gao, J., Wang, W.Y., Mao, Y.W., Gräff, J., Guan, J.S., Pan, L., Mak, G., Kim, D., Su, S.C., and Tsai, L.H. (2010). A novel pathway regulates memory and plasticity via SIRT1 and miR-134. Nature *466*, 1105–1109.

16. Gaughwin, P., Ciesla, M., Yang, H., Lim, B., and Brundin, P. (2011). Stage-specific modulation of cortical neuronal development by *Mmu-miR-134*. Cereb. Cortex *21*, 1857–1869.

17. Elmén, J., Lindow, M., Schütz, S., Lawrence, M., Petri, A., Obad, S., Lindholm, M., Hedtjärn, M., Hansen, H.F., Berger, U., et al. (2008). LNA-mediated microRNA silencing in non-human primates. Nature *452*, 896–899.

18. Jimenez-Mateos, E.M., Engel, T., Merino-Serrais, P., Fernaud-Espinosa, I., Rodriguez-Alvarez, N., Reynolds, J., Reschke, C.R., Conroy, R.M., McKiernan, R.C., deFelipe, J., and Henshall, D.C. (2015). Antagomirs targeting microRNA-134 increase hippocampal pyramidal neuron spine volume in vivo and protect against pilocarpine-induced status epilepticus. Brain Struct. Funct. *220*, 2387–2399.

19. Straarup, E.M., Fisker, N., Hedtjärn, M., Lindholm, M.W., Rosenbohm, C., Aarup, V., Hansen, H.F., Ørum, H., Hansen, J.B., and Koch, T. (2010). Short locked nucleic acid antisense oligonucleotides potently reduce apolipoprotein B mRNA and serum cholesterol in mice and non-human primates. Nucleic Acids Res. *38*, 7100–7111.

20. van Vliet, E.A., da Costa Araújo, S., Redeker, S., van Schaik, R., Aronica, E., and Gorter, J.A. (2007). Blood-brain barrier leakage may lead to progression of temporal lobe epilepsy. Brain *130*, 521–534.

21. Shlosberg, D., Benifla, M., Kaufer, D., and Friedman, A. (2010). Blood-brain barrier breakdown as a therapeutic target in traumatic brain injury. Nat. Rev. Neurol. *6*, 393–403.

22. Lublinsky, S., Major, S., Kola, V., Horst, V., Santos, E., Platz, J., Sakowitz, O., Scheel, M., Dohmen, C., Graf, R., et al. (2019). Early blood-brain barrier dysfunction predicts neurological outcome following aneurysmal subarachnoid hemorrhage. EBioMedicine *43*, 460–472.

23. Rüber, T., David, B., Lüchters, G., Nass, R.D., Friedman, A., Surges, R., Stöcker, T., Weber, B., Deichmann, R., Schlaug, G., et al. (2018). Evidence for peri-ictal blood-brain barrier dysfunction in patients with epilepsy. Brain *141*, 2952–2965.

24. Jimenez-Mateos, E.M., Arribas-Blazquez, M., Sanz-Rodriguez, A., Concannon, C., Olivos-Ore, L.A., Reschke, C.R., Mooney, C.M., Mooney, C., Lugara, E., Morgan, J., et al. (2015). microRNA targeting of the P2X7 purinoceptor opposes a contralateral epileptogenic focus in the hippocampus. Sci. Rep. *5*, 17486.

25. Michalak, Z., Sano, T., Engel, T., Miller-Delaney, S.F., Lerner-Natoli, M., and Henshall, D.C. (2013). Spatio-temporally restricted blood-brain barrier disruption after intra-amygdala kainic acid-induced status epilepticus in mice. Epilepsy Res. *103*, 167–179.

26. Keaney, J., Walsh, D.M., O'Malley, T., Hudson, N., Crosbie, D.E., Loftus, T., Sheehan, F., McDaid, J., Humphries, M.M., Callanan, J.J., et al. (2015). Autoregulated paracellular clearance of amyloid-β across the blood-brain barrier. Sci. Adv. *1*, e1500472.

27. Li, T., Ren, G., Lusardi, T., Wilz, A., Lan, J.Q., Iwasato, T., Itohara, S., Simon, R.P., and Boison, D. (2008). Adenosine kinase is a target for the prediction and prevention of epileptogenesis in mice. J. Clin. Invest. *118*, 571–582.

28. Jiang, X., Lachance, M., and Rossignol, E. (2016). Involvement of cortical fast-spiking parvalbumin-positive basket cells in epilepsy. Prog. Brain Res. *226*, 81–126.

29. Buono, R.J., Lohoff, F.W., Sander, T., Sperling, M.R., O'Connor, M.J., Dlugos, D.J., Ryan, S.G., Golden, G.T., Zhao, H., Scattergood, T.M., et al. (2004). Association between variation in the human KCNJ10 potassium ion channel gene and seizure susceptibility. Epilepsy Res. *58*, 175–183.

30. Akarsu, E.S., Mamuk, S., and Comert, A. (1998). Inhibition of pentylenetetrazol-induced seizures in rats by prostaglandin D_2. Epilepsy Res. *30*, 63–68.

31. Iwasa, K., Yamamoto, S., Yagishita, S., Maruyama, K., and Yoshikawa, K. (2017). Excitotoxicity-induced prostaglandin D_2 production induces sustained microglial activation and delayed neuronal death. J. Lipid Res. *58*, 649–655.

32. Liang, X., Wu, L., Hand, T., and Andreasson, K. (2005). Prostaglandin D_2 mediates neuronal protection via the DP1 receptor. J. Neurochem. *92*, 477–486.

33. Gross, C., Yao, X., Engel, T., Tiwari, D., Xing, L., Rowley, S., Danielson, S.W., Thomas, K.T., Jimenez-Mateos, E.M., Schroeder, L.M., et al. (2016). MicroRNA-mediated downregulation of the potassium channel Kv4.2 contributes to seizure onset. Cell Rep. *17*, 37–45.

34. Morris, G., Brennan, G.P., Reschke, C.R., Henshall, D.C., and Schorge, S. (2018). Spared CA1 pyramidal neuron function and hippocampal performance following antisense knockdown of microRNA-134. Epilepsia *59*, 1518–1526.

35. Sambandan, S., Akbalik, G., Kochen, L., Rinne, J., Kahlstatt, J., Glock, C., Tushev, G., Alvarez-Castelao, B., Heckel, A., and Schuman, E.M. (2017). Activity-dependent spatially localized miRNA maturation in neuronal dendrites. Science *355*, 634–637.

36. Wetherington, J., Serrano, G., and Dingledine, R. (2008). Astrocytes in the epileptic brain. Neuron *58*, 168–178.

37. Janssen, H.L., Reesink, H.W., Lawitz, E.J., Zeuzem, S., Rodriguez-Torres, M., Patel, K., van der Meer, A.J., Patick, A.K., Chen, A., Zhou, Y., et al. (2013). Treatment of HCV infection by targeting microRNA. N. Engl. J. Med. *368*, 1685–1694.

38. Wang, X., Luo, Y., Liu, S., Tan, L., Wang, S., and Man, R. (2017). MicroRNA-134 plasma levels before and after treatment with valproic acid for epilepsy patients. Oncotarget *8*, 72748–72754.

39. McArdle, H., Jimenez-Mateos, E.M., Raoof, R., Carthy, E., Boyle, D., ElNaggar, H., Delanty, N., Hamer, H., Dogan, M., Huchtemann, T., et al. (2017). "TORNADO" – Theranostic One-Step RNA Detector; microfluidic disc for the direct detection of microRNA-134 in plasma and cerebrospinal fluid. Sci. Rep. *7*, 1750.

40. Kullmann, D.M., Schorge, S., Walker, M.C., and Wykes, R.C. (2014). Gene therapy in epilepsy—is it time for clinical trials? Nat. Rev. Neurol. *10*, 300–304.

41. Schindelin, J., Arganda-Carreras, I., Frise, E., Kaynig, V., Longair, M., Pietzsch, T., Preibisch, S., Rueden, C., Saalfeld, S., Schmid, B., et al. (2012). Fiji: an open-source platform for biological-image analysis. Nat. Methods *9*, 676–682.

42. van Wageningen, S., Kemmeren, P., Lijnzaad, P., Margaritis, T., Benschop, J.J., de Castro, I.J., van Leenen, D., Groot Koerkamp, M.J., Ko, C.W., Miles, A.J., et al. (2010). Functional overlap and regulatory links shape genetic interactions between signaling pathways. Cell *143*, 991–1004.

43. Jassal, B., Matthews, L., Viteri, G., Gong, C., Lorente, P., Fabregat, A., Sidiropoulos, K., Cook, J., Gillespie, M., Haw, R., et al. (2020). The reactome pathway knowledgebase. Nucleic Acids Res. *48* (D1), D498–D503.

44. R Core Team (2020). R: a language and environment for statistical computing, https://www.R-project.org/.

45. Yu, G., and He, Q.Y. (2016). ReactomePA: an R/Bioconductor package for reactome pathway analysis and visualization. Mol. Biosyst. *12*, 477–479.

46. Yu, G., Wang, L.G., Han, Y., and He, Q.Y. (2012). clusterProfiler: an R package for comparing biological themes among gene clusters. OMICS *16*, 284–287.

47. Vuokila, N., Aronica, E., Korotkov, A., van Vliet, E.A., Nuzhat, S., Puhakka, N., and Pitkänen, A. (2020). Chronic regulation of miR-124-3p in the perilesional cortex after experimental and human TBI. Int. J. Mol. Sci. *21*, 2418.

48. Almeida Silva, L.F., Reschke, C.R., Nguyen, N.T., Langa, E., Sanz-Rodriguez, A., Gerbatin, R.R., Temp, F.R., de Freitas, M.L., Conroy, R.M., Brennan, G.P., et al. (2020). Genetic deletion of microRNA-22 blunts the inflammatory transcriptional response to status epilepticus and exacerbates epilepsy in mice. Mol. Brain *13*, 114.